Nanoscale

Accepted Manuscript

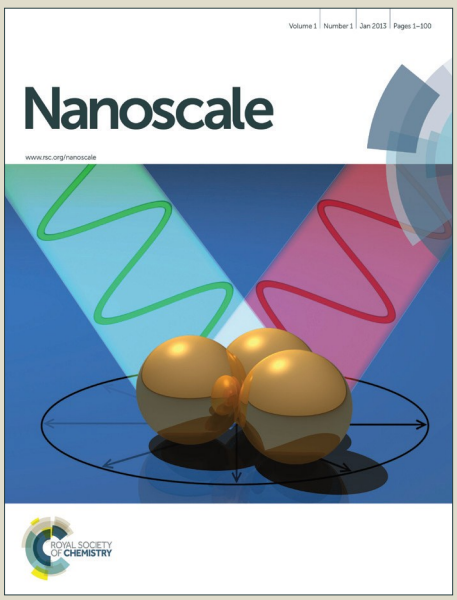

ROYAL SOCIETY OF CHEMISTRY

www.rsc.org/nanoscale

Nanoscale

ARTICLE

Nanoscale direct mapping of localized and induced noise sources on conducting polymer films

Received 13th July 2015,
Accepted 00th January 2015

DOI: 10.1039/x0xx00000x

www.rsc.org/

Shashank Shekhar,† Duckhyung Cho,† Hyungwoo Lee, Dong-guk Cho and Seunghun Hong*

The localized noise-sources and those induced by external-stimuli were directly mapped by a conducting-AFM integrated with custom-designed noise measurement set-up. In this method, current and noise images of a Poly(9,9-dioctylfluorene)-polymer-film on a conducting-substrate were recorded simultaneously, enabling the mapping of the resistivity and noise source density (N_T). The polymer-films exhibited separate regions with *high* or *low* resistivities, which were attributed to the *ordered* or *disordered* phases, respectively. A larger number of noise-sources were observed in the disordered-phase-regions than in the ordered-phase regions, due to structural disorderings. *Increased bias-voltages* on the disordered-phase-regions resulted in *increased* N_T, which is explained by the structural deformation at high bias-voltages. On photo-illuminations, the ordered-phase-regions exhibited rather large increase in the conductivity and N_T. Presumably, the illumination released carriers from deep-traps which should work as additional noise-sources. These results show that our methods provide valuable insights about noise-sources and, thus, can be a powerful tool for basic research and practical applications of conducting polymer films.

1 Introduction

A current noise is one of the most important parameters that determines the performance of electronic devices[1-14] based on various materials such as conducting polymers,[10-14] graphene,[1,6-8] quantum dots,[3] molecular wires,[4,5] carbon nanotubes,[9] and transition metal dichalcogenides.[2] Furthermore, the analysis of such electronic noises can provide a valuable information about basic materials properties such as structures,[13] defects,[14] impurities[7] and inhomogeneities.[8] For example, although conducting polymer-based devices have been extensively utilized for versatile optoelectronic applications,[15,16] the performances of such devices are still poor compared with those of semiconductor-based devices partly due to various localized defects such as structural disorders, variations of conjugation lengths, domain boundaries, and grain boundaries. Such defects in conducting polymer-based devices can adversely affect electrical conductions and generate electrical noises[13,15,17-22] and, eventually, degrade their device performances such as channel mobilities, off currents, luminescence efficiencies and operating voltages.[11,17,23] Thus, it is essential to understand the electrical noise sources to develop high performance devices based on conducting polymers. However, previous studies about electrical noise sources often relied on extensive statistical analysis of many electrical measurements data from multiple devices, which can be an extremely time-consuming task and can still provide only indirect evidences about possible localized noise sources.[20,21,24-26] And, it has been very difficult, if not impossible, to directly image localized noise sources or map the distribution of resistivity in electrical channels.[22]

Herein, we developed a method to directly map the distribution of localized noise sources and those generated by external stimuli on conducting polymer films. In this work, a nanoscale conducting probe installed in a conducting atomic force microscope (AFM) made a direct contact with a Poly(9,9-dioctylfluorene) (PFO) polymer film, and the maps of electrical currents and noise power spectral density (PSD) were measured simultaneously, allowing one to estimate the distributions of charge carriers and noise sources generated by various external stimuli such as bias voltages and lights. In the PFO polymer films, we found two separate regions with rather *high* or *low* resistivity values, which were attributed to polymer regions with *ordered crystalline* or *disordered* phases. The disordered-phase regions with a higher resistivity exhibited a higher density of noise sources than the ordered-phase regions, presumably due to the structural disorderings in the regions. Interestingly, an *increased bias voltage* on the disordered-phase regions resulted in an *increased conductivity* as well as *increased noise source density*. A plausible explanation is that the high bias voltage allowed charge carries to overcome conduction barriers and, thus, increased the channel conductivity, while the increased charge carriers at a high bias voltage condition could also increase lattice distortions and structural defects in polymer chains, resulting in increased noise source densities. On the illumination of lights, the ordered-phase regions exhibited rather large increase in the conductivity and noise source density. Presumably, the light illumination released some charge carriers trapped in rather deep traps. Thus, the released *charge carriers* and such *deep traps* should work as *photo-carriers* and additional *noise sources,* respectively. These results show that our method can provide valuable insights about the generation of noises in conducting polymer channels. Thus, our strategy can be a powerful tool for basic research about electrical noises and practical applications based on conducting polymer devices.

Department of Physics and Astronomy, and Institute of Applied Physics, Seoul National University, Seoul Korea 151-747.
** E-mail: seunghun@snu.ac.kr*
† Equally contributing authors.
Electronic Supplementary Information (ESI) available:
See DOI: 10.1039/x0xx00000x

2 Experimental Section

2.1 Device fabrication

Firstly, the PEDOT:PSS solution (supplied by Sigma-Aldrich, product ID 483095, conductivity ~ 1 S/cm) was spin coated on an ITO

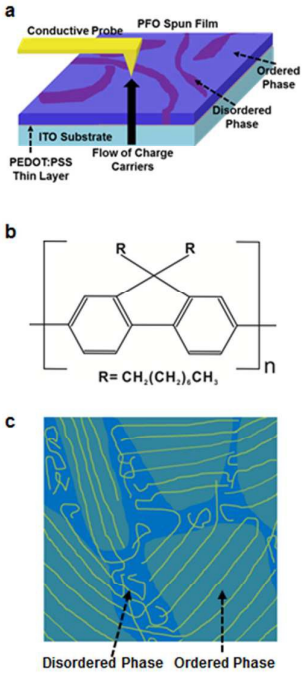

Fig. 1 Schematic diagram showing the scanning noise measurement set-up and the structure of a PFO polymer film. (a) Schematic diagram depicting noise measurement set-up for a PFO polymer film on an ITO/PEDOT:PSS substrate. The PFO film was comprised of the different phases and domains. A small dc bias was applied between the ITO and the AFM probe. The currents and noise signals were measured by a home-built network analyser capable of measuring the signals in the real time at different locations of the probe on the polymer film. (b) Chemical structure of PFO polymer. (c) Schematic diagram depicting the ordered and disordered phases of PFO in the thin film configuration.

substrate with the 6000 rpm and baked at 150 ^{o}C for 30 minutes. By this process, we could obtain a thin PEDOT:PSS coating with a rather uniform thickness of ~ 10nm and a homogeneous high electrical conduction.[27,28] The PFO polymer was purchased from Sigma-Aldrich (Product ID 571652, M_W < 20000). 10 mg of the PFO polymer was dissolved in 10 ml of chloroform ($CHCl_3$) by applying a sonication at 60 ^{o}C for 90 minutes. The prepared PFO solution was spin coated on the PEDOT:PSS-coated ITO substrate at the 4000 rpm for 60 seconds. The thickness of the film was ~ 100 nm as measured by AFM. The film was heated at 80 ^{o}C for 15 minutes.

2.2 Scanning noise measurement set-up

Fig. 1a shows a schematic diagram of our current and noise measurement set-up with a PFO film on an ITO/PEDOT:PSS substrate. The PFO is one of the most widely used polymers due to its high mobility, high electroluminescence efficiency and a wide band gap.[29,30] For the current and noise measurements, a platinum (Pt) tip (25Pt300B, Park Systems) installed on a conducting AFM (XE-70, Park Systems) made a direct contact with the surface of the spun PFO film on the ITO/PEDOT:PSS substrate. Then, a dc bias (0.2 V) was applied between the ITO and the Pt tip by a function generator (DS345, Stanford Research Systems). The electrical currents through the probe were measured and converted to amplified voltage signals by a low-noise preamplifier (SR570, Stanford Research Systems). Simultaneously, the noise PSD of the signals with a specific frequency was measured by a homemade custom-designed spectrum analyser.[31] To measure the noise signals, we used a band-pass filter (6 dB) of the SR570 preamplifier. The noise PSD was collected in the entire width of a band. We obtained the absolute noise PSD value at the central frequency of the band, by dividing the total noise PSD to the bandwidth of the filter. Using this system, we could obtain the maps of the topography, the current and the noise PSD with a specific frequency on the PFO film, simultaneously. For the light illumination during the AFM measurements a solar spectrum system (Newport 91160A, power density of 100 mW/cm^2) was utilized. All AFM measurements were performed under ambient conditions in a closed box to avoid stray lights which could degrade the polymer.[32] The measurements were repeated at least 5 times to confirm the reproducibility. Finally, the measured PSD maps were analysed using an empirical model to obtain noise characteristic parameters such as noise source densities in the PFO film. Considering that it has been very difficult to directly identify noise sources in a polymer film, the direct imaging capability of noise sources via our strategy can be a major breakthrough in noise research about conducting polymers.

2.3 Structure of the PFO polymer

Fig. 1b shows the chemical structure of the PFO polymer. The monomer unit of PFO is a conjugated molecule (fluorene) where two benzene rings are linked in a way providing conjugation across the molecule (as can be seen in the Fig. 1b). Consequently, a reduced band gap and delocalized excited state molecular orbitals can be observed in the PFO. Fig. 1c shows a schematic diagram of the microstructure of a PFO film.[15] In a semi-crystalline conducting polymer such as a PFO, *ordered* and *disordered* phases can coexist.[15,19,33] The ordered-phases which are comprised of aggregates,[34] β-phases[33] and planar configurations[35] look like fringed micelles and disordered-phases look like entangled polymer chains.[18] The extra-long polymer chains provide the connectivity between the ordered phases.[18]

3 Results and Discussion

3.1 Identification of domains and phases of the polymer film

Fig. 2a shows an AFM topography image of a PFO thin film on an ITO/PEDOT:PSS substrate. The film was spun from the PFO solution in chloroform. The image shows the polymer film was comprised of many separated domains and their boundaries which appeared as hairline cracks (few nm wide), as reported previously.[26,36] One of such domains was marked with a green line along its boundary. The average domain size was ~ 200 nm, which is consistent with previous reports.[15,26]

Fig. 2b is a current map measured on the PFO film. The applied bias was 0.2 V. For clarity, the domain was marked with a green line along its boundary. The current image shows a variation in currents inside the domain. A clear contrast between a high current (~ 10^{-5} A) area (marked with yellow line) and a low current (~ 10^{-7} A) area (marked with blue line) was visible in the domain. As a control experiment, we also performed the current mapping on the PEDOT:PSS film on ITO without PFO (see Fig. S1 in the supplementary information). The current image shows homogeneous distribution of currents and the current levels much higher than those on the PFO-coated film.[27] Hence, the

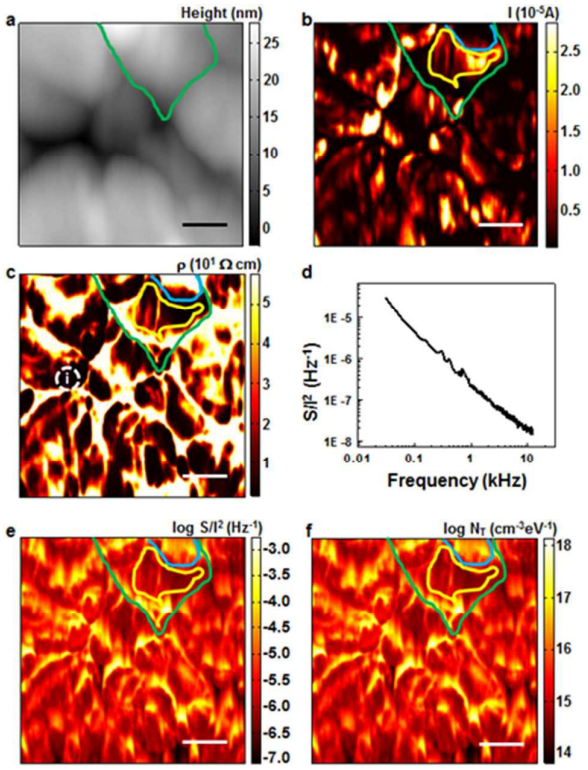

Fig. 2 Mapping resistivity and noise source density of the polymer film. (a) Contact mode AFM topography image of a PFO film. The domains and domain boundaries are observed in the topography image of the film. A domain is marked with a green line. The average domain size was ~ 200 nm. (b) Current map showing local variation in currents within the domains. The domains have two phases with *high* and *low* currents marked with *yellow* and *blue* lines, respectively. (c) Resistivity map showing the presence of two phases in the domains. The resistivity of the domain boundaries was distinctively high. (d) Current normalized noise PSD dependence on frequencies. It shows a typical *1/f* behaviour. (e) Noise PSD map on a log-scale. The PSD of noise was high in the disordered phase as compared to the ordered phase. The domain boundaries exhibited a rather high noise PSD. (f) Noise source density map showing the existence of a large number of noise-sources in the disordered-phase regions. The noise source densities in the ordered phase were ~ 10^{14}-10^{15} cm^3eV^{-1}, and those in the disordered phase were ~ 10^{16}-$10^{17.5}$ cm^3eV^{-1}. The domain boundary showed noise source density of ~ $10^{17.5}$ cm^3eV^{-1}. Scale bars are 200 nm.

ITO/PEDOT:PSS substrate could have provided homogeneous charge injections throughout the sample, and the current variations on the PFO-coated sample originated mainly from the PFO film. The *high* and *low* currents regions can be attributed to the *ordered* and *disordered* -phase regions of the polymer, respectively.[33,37] The typical size of the ordered and disordered-phases was in the range of ~ 10-100 nm, which was similar to the values reported by other methods.[15] The ordered-phase of a polymer was reported to consist of planar polymer chains, β-phases and aggregates which should have helped the charge conduction and enhance the conduction of ordered-phase polymer structures.[33,37] The lateral force microscopy images show that disordered regions with a lower conductivity exhibited larger lateral forces than the ordered regions, which could be attributed to a rather large surface energy and roughness of the disordered regions as reported previously (see Fig. S2 in the supplementary information).[38,39]

3.2 Two-dimensional resistivity mapping of the polymer film

The map of resistivity (Fig. 2c) was calculated from the current map considering a vertical transport. The details of the calculation are described in the next section (3.3). In brief, we assumed a vertical charge transport from the underlying ITO electrode, to the conducting probe through the polymer layer. In common conducting AFM measurements, the effective contact area of the probe on the polymer may vary depending on probes and is an uncertain parameter. In our work, the contact area was estimated by using it as a fitting parameter so that the averaged resistivity value calculated from the current map is the same as previously-reported resistivity value of bulk polymer films.[40,41] For example, the effective contact area A_{eff} estimated from the current map in Fig. 2b was ~ 1900 nm^2, which is consistent with the approximate probe diameter of ~ 25 nm provided by the manufacturer. Using the estimated effective contact area, we could obtain the localized resistivity map of the polymer film (Fig. 2c). The resistivity map also shows *ordered* or *disordered* phases inside individual domains, which are marked by *yellow* and *blue* lines. The ordered phase had the resistivity ρ of 0.5 Ω-cm whereas the disordered phase showed a rather large resistivity ρ of 50 Ω-cm, which are consistent with the previously-reported values.[40,41] The domain boundaries showed a distinctively high resistivity (ρ > 50 Ω-cm). The high resistivity on domain boundaries could be attributed to high disorderness of the polymer at the boundaries.

3.3 Calculation method of the resistivity of polymer films on the conducting substrate

Since the resistivity of the polymer was rather high, we can assume that the charge carriers flow mainly in a vertical direction from the underlying ITO substrate, to the conducting probe through the polymer layer and the parasitic currents in a lateral direction inside the polymer film should be limited. Thus, we calculated the resistivity of the polymer assuming a vertical charge transport from the underlying electrode to the conducting probe through the polymer film. In this case, the resistivity ρ of the polymer can be written like $\rho = A_{eff}R/d$, where A_{eff}, R, and d represent the effective contact area of the conducting probe, measured resistance, and the thickness of the polymer film, respectively. In our experiment, the thickness of the polymer film was d ~ 100 nm. R varies depending on the location of the conducting probe on the polymer. For example, the current map shows high (or low) resistance values

Table 1

	A_{eff} (nm^2)	r_{eff} (nm)
Fig. 2	1900	24.66
Fig. 3	2544	28.46
Fig. 4	1721	23.41

when the conducting probe was located on disordered (or order) phase regions. In our measurement, the effective contact area A_{eff} of the probe is still uncertain and may vary depending on different probes. Here, we first calculated the averaged resistance R_{avg} from a current map. Then, the effective contact area A_{eff} was estimated by using it as a fitting parameter so that the averaged resistivity $\rho_{avg} = A_{eff} R_{avg}/d$ calculated from R_{avg} is the same as the previously-reported resistivity value $\rho_{bulk} \sim 10^2\,\Omega$–cm of bulk polymer films.[40,41] Using the estimated effective contact area A_{eff} and a current map, we could calculate a map showing the variation of localized resistivity of a polymer film. Since the effective contact area A_{eff} varies from measurement to measurement, we calculated the effective area for each data set. Table 1 shows the A_{eff} for the data in Figs. 2, 3, and 4. The effective radius r_{eff} of the probe is calculated from A_{eff} by assuming a circular contact area. Note that the estimated effective radii are similar to the actual radius of our probe (~ 25 nm).

3.4 Noise PSD and noise source density mapping of the polymer films

Fig. 2d shows the log-log plot of current-normalized noise PSD vs frequencies in a polymer domain. For this measurement, we kept the probe stationary at a designated position (as marked by "i" in Fig. 2c). The slope of the curve was ~ 1, indicating a *1/f* noise behaviour below ~ 10 kHz. This behaviour is consistent with the previously observed *1/f* noise behaviours in polymers.[11,12,14,42] Previous studies suggested that such *1/f* noise in a polymer film mainly originates from the trapping and detrapping of charge carriers by trap states in the film.[12,40,42,43] A single noise source with a specific relaxation time generates a Lorentzian-shaped noise spectrum. However, if multiple noise sources with different relaxation times existed in a polymer film, the noise PSD of the different noises sources were average out, resulting in the noise spectra proportional to *1/f*. The observed *1/f* behaviour implies that we can analyse our noise image data to estimate the noise source density, after assuming that the electrical noises in our system were generated by multiple noise sources between the substrate and the conducting AFM probe.

Fig. 2e shows the map of the noise PSD (S/I^2) measured at a central frequency of 548 Hz. The disordered-phase regions with a rather high resistivity exhibited high PSD values of ~ 10^{-5} to 10^{-3} Hz^{-1}, while the ordered phases exhibited a rather low PSD of ~ $10^{-6.5}$ to 10^{-5} Hz^{-1}. These results implicate that structures of polymer films can significantly affect their noise characteristics. For example, the entangled polymer chains in disordered phases of the polymer could act as noise sources.[19,37] The domain boundaries exhibited a rather high PSD, which was comparable to that in the disordered-phases.

The measured maps of the noise PSD and currents can be utilized to calculate the map of noise source density N_T in the polymer film. In brief, we assumed that the electrical noise was generated by charge traps during a vertical charge transport directly from the ITO substrate to the conducting probe, through the polymer film. Then, the PSD of the mean-square fluctuation in the number of occupied charge traps in the small segment of the polymer film within the contact area *A* of the probe can be written as [44,45]

$$N_T(x,y) = \Delta S_I(f,x,y)\frac{(\Delta C)^2}{(I)^2}\cdot\frac{1}{A\cdot d\cdot kT}\cdot\frac{1+[2\pi f\cdot\tau(x,y)]^2}{4\tau(x,y)} \quad (1)$$

where ΔC is the carrier number in the segment of the polymer, τ is the average trapping time, and d is the thickness of the polymer. The detail calculations of the noise source density N_T are described in the section 3.5.

Fig. 2f shows the noise source density map calculated from the measured noise PSD and current maps. The noise source density in the ordered phase was estimated as ~ 10^{14}-10^{15} $cm^{-3}eV^{-1}$, whereas that in the disordered phase was ~ 10^{16}-10^{18} $cm^{-3}eV^{-1}$. A plausible explanation can be that entangled polymer chains in disordered-phase regions could produce structural defects, resulting in the high noise source density.[19,37] The noise source density obtained here is in good agreement with previously-reported trap densities (~ 10^{17} $cm^{-3}eV^{-1}$) in conducting polymers.[20] At the domain boundaries, the noise source density was of ~ 3×10^{17} $cm^{-3}eV^{-1}$. The high noise source density at the boundaries could be attributed to the high disorderness of the polymer at the boundary regions.[18] These results clearly show that the nanoscale disorders of polymer chains not only increase the resistivity but also generate significant amount of electrical noises.

3.5 Estimation of the noise source density in polymer films

In this measurement, electrical currents flew vertically between the conducting AFM tip and the underlying ITO films. Thus, the majority of electrical noises should be generated by the noise sources inside the small volume of the polymer film between the ITO electrode and the conducting AFM tip. Then, the PSD of the mean-square fluctuation in the number of occupied charge traps in the small segment of the polymer film within the contact area A of the tip can be written as [44,45]

$$\Delta S_{N_T}(f,x,y) = A\cdot\int_{-\infty}^{\infty}\int\frac{4\tau(E,x,y,z)}{1+[2\pi f\cdot\tau(E,x,y,z)]^2}\cdot f_t(1-f_t)\cdot N_T(E,x,y,z)\cdot dz\cdot dE \quad (2)$$

where the N_T, τ, and *f* are *the density of charge traps* over the space and energy, *a trapping time constant*, and *a frequency*, respectively. The integral over *z* ranged from *0* to the polymer thickness *d*. The trap occupancy function can be written as $f_t(E) = [1 + \exp\{(E - E_f)/kT\}]^{-1}$ where E_f is Fermi level. At a rather low temperature condition including a room temperature, $f_t(1\text{-}f_t)$ behaves like a delta function around the Fermi level E_f, and the equation (2) after the integral over *E* can be simplified as [46]

$$\Delta S_{N_t}(f,x,y) = A\cdot kT\cdot\int\frac{4\tau(E_f,x,y,z)}{1+[2\pi f\cdot\tau(E_f,x,y,z)]^2}\cdot N_T(E_f,x,y,z)\cdot dz \quad (3)$$

Assuming that charge traps are distributed uniformly over the *z* direction, the equation (3) can be approximated as

$$\Delta S_{N_t}(f,x,y) = A\cdot d\cdot kT\cdot N_T(x,y)\frac{4\tau(x,y)}{1+[2\pi f\cdot\tau(x,y)]^2} \quad (4)$$

The noise PSD ΔS_I can be written as

$$\Delta S_I(f,x,y) = \frac{(I)^2}{(\Delta C)^2}\Delta S_{N_t}(f,x,y) \quad (5)$$

where ΔC is the carrier number in the segment of the polymer. Then, the noise source density N_T can be written like,

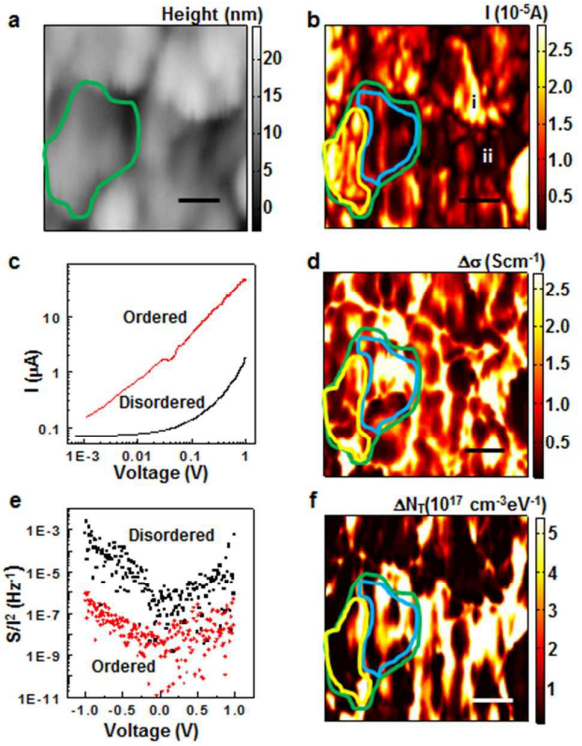

Fig. 3 Voltage induced noise generation in polymer film. (a) Topography image of a PFO polymer film. A domain is marked by a green line. (b) Current map of the PFO polymer film. Within the marked domain, different phases of the polymer are seen (marked by yellow and blue lines). (c) *I-V* curves of an ordered and disordered phase of the polymer film. The *I-V* curve of the ordered phase was nearly linear. The disordered phase showed a slow increase (less than linear) in current at a low bias which increased rapidly above 0.1 V. (d) Map showing the change of the conductivity when the bias voltage was increased from 0.1 V to 1 V. The disordered regions exhibited much larger increase in the conductivity than the ordered regions. (e) Noise PSD (S/I^2) versus bias plots measured at the ordered and disordered regions. The PSD increased with the increased bias voltages. (f) Map showing the change in the noise source densities when the bias voltage was increased from 0.1 V to 1 V. The disordered-phase regions exhibited a much larger increase of the noise source density than ordered-phase regions. Scale bars are 200 nm.

$$N_T(x,y) = \Delta S_I(f,x,y)\frac{(\Delta C)^2}{(I)^2}\cdot\frac{1}{A\cdot d\cdot kT}\cdot\frac{1+[2\pi f\cdot\tau(x,y)]^2}{4\tau(x,y)} \quad (6)$$

The average trapping time τ and the carrier density in the conducting polymer were reported as ~ 10^{-2} seconds and ~ 10^{17} cm^{-3}, respectively.[43,47] The thickness of the polymer film was ~ 100 nm. The contact area A (1900 nm^2) was estimated by using it as a fitting parameter so that the averaged resistivity calculated from the current map is the same as the previously-reported resistivity value of bulk polymer films.[40,41]

3.6 Voltage induced noise generation in polymer films

A high electric field in polymer materials can affect their electrical conductivity σ and noise characteristics (Fig. 3).[42,43] Fig. 3a, and b shows the topography and current images of the same region on a PFO film. The *ordered* or *disordered* phases in a single domain (marked by green line) were marked by *yellow* or *blue* lines, respectively. Fig. 3c shows the graph of typical *I-V* measurement results on the ordered (marked by (i) in Fig. 3b) and disordered (marked by (ii) in Fig. 3b) phase regions. The *I-V* curve on an ordered-phase region was nearly linear, while that on a disordered-phase region exhibited a rapid increase of its conductivity with the increase of a bias voltage above ~ 0.1 V. In order to estimate the effect of electric fields on the conductivity σ, we mapped the conductivity values at the bias voltages of 1 and 0.1 V (Fig. S3 in supplementary information) and estimated the difference $\Delta\sigma = [\sigma(1V) - \sigma(0.1V)]$ (Fig. 3d). The conductivity changes on the *ordered* and *disordered* phase regions were ~ *0.2* and ~ *2.3* Scm^{-1}, respectively. Presumably, the structural defects in the disordered region worked as a conduction barrier for the charge carriers at a rather low bias voltage.[47] However, the high bias voltage above 0.1 V allowed charge carries to overcome the conduction barriers in the disordered-phase regions and, thus, increased the charge injection and the channel conductivity.

Fig. 3e shows the graph of noise PSD (S/I^2 at 548 Hz) vs a bias voltage on the ordered and disordered phase regions. The PSD increased with the increase in the bias for all voltages. To estimate the change in the noise source densities, we mapped the noise source density N_T at bias voltages of 1 V and 0.1 V and calculated the map of noise source density change $\Delta N_T = [N_T(1V) - N_T(0.1V)]$ (Fig. 3f). Overall, ΔN_T had positive values indicating that the increase of the noise source density in the polymer at a high bias. Interestingly, the noise source density increased by ΔN_T ~ 5×10^{17} $cm^{-3}eV^{-1}$ on the disordered-phase regions with a rather large $\Delta\sigma$, while other regions exhibited a rather small change of ΔN_T ~ 1×10^{17} $cm^{-3}eV^{-1}$. This result indicates that the noise source density increased more in the disordered-phase regions which had a rather large enhancement of their conductivity. Presumably, the charge injected at a high bias voltage distorts disordered polymer phases more easily and induced more defects and distortions than in ordered-phase regions.[48]

3.7 Mapping of photo-generated conductivity and noise in polymer films

We studied the effect of the light illumination on the electrical currents and noises in a PFO polymer film (Fig 4). For light illumination, we used a solar spectrum system whose power density was 100 mW/cm^2. The light was vertically illuminated on the surface of the polymer film from the top side with a help of an optical cable. Fig 4*a* and b show the *topography* and *current* images of a PFO film, respectively. For an eye guideline, a *domain*, an *ordered-phase region*, and a *disordered-phase region* are marked with the *green*, *yellow* and *blue* lines, respectively. When a light was illuminated on the film, the polymer film exhibited increased currents, presumably, due to the generation of photo-carriers (Fig. 4c). Note that the current was mainly enhanced in the ordered-phase regions in the order of μA range. The disordered-phase regions and domain boundaries contributed very little to the photo-excitation currents (~ nA range). Fig. 4d shows the map of conductivity change $\Delta\sigma$ upon illumination. The average conductivity change was 15 Scm^{-1} whereas its peak value was ~ 25 Scm^{-1}. The result shows a significant increase in the conductivity on

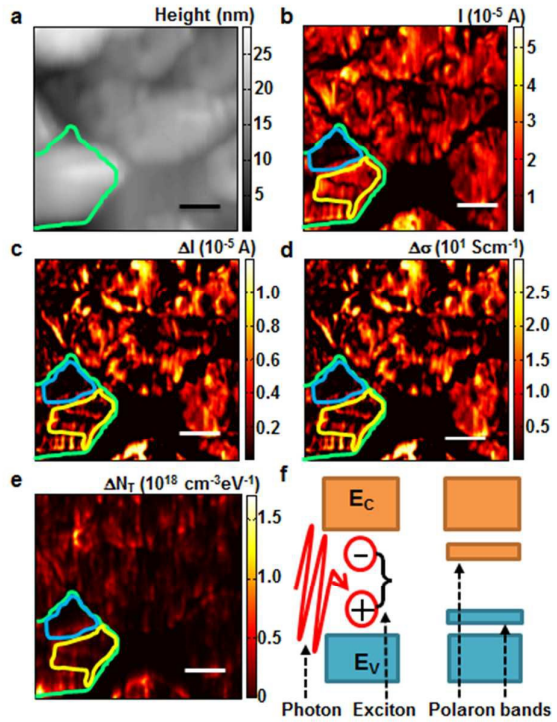

Fig. 4 Photoexcitation noise in the polymer film. (a) Topography image of a PFO film. A domain is marked with a green line. (b) Current map of the PFO film measured under a light illumination. The applied bias was 0.2 V. (c) Photo-generated current map which was recorded as a difference in the illuminated current to the dark current. The currents in the ordered-phase regions with rather higher conductivities increased much more than those in the disordered-phase regions or domain boundaries. (d) Map of the conductivity change after the light illumination. The ordered-phase regions exhibited much larger change in conductivity than disordered-phase regions. (e) Map showing the change of noise source densities after the light illumination. A larger increase of the noise source densities was observed in the ordered-phase regions than those in the disordered-phase regions, which could be attributed to the structural distortion of PFO lattice structures due to the generated photo-carriers. (f) Schematic diagrams showing exciton generations in PFO under a light illumination, resulting in polaron bands. These bands may act as additional noise sources and, thus, increase electrical noises. Scale bars are 200 nm.

the ordered-phase regions. Presumably, although there could be some photo-carrier generation in disordered-phase regions, the generated photo-carriers could not result in the significant increase of electrical currents due to the shorter diffusion length and the high noise source density in the disordered-phase regions.

The light illumination also enhanced the electrical noises (Fig. S4 in supplementary information). Interestingly, we found that the increase of PSD in the ordered-phase regions with a rather high conductivity was larger by several times than that in the disordered regions. Fig. 4e shows the change of estimated noise source density ΔN_{TL} upon the illumination. Note that there was an increase in ΔN_{TL} on the ordered-phase regions where rather large photocurrents were generated. The increased amount of the noise source density in the ordered-phase regions was of ~ 4×10^{17} $cm^{-3}eV^{-1}$, which was much larger than that in the disordered phases. One plausible explanation can be a structural distortion due to the generated photo-carriers (Fig. 4f).[16] The light illumination induced the generation of photo-carriers which formed excitons in the ordered regions of the polymer. The generated excitons could locally distort the lattice and form polarons, which could lead to new gap states.[48,49] Such a gap state can work as charge traps, generating electrical noises.

Conclusions

In summary, we developed a strategy to directly map the generation of noise-sources induced by external stimuli such as electric fields and lights on a polymer thin film. Our results show that a PFO film was comprised of ordered-phase regions with a rather low resistivity and disordered ones with a high resistivity. The ordered-phase regions exhibited lower noise source densities as compared to those of disordered-phase regions. Interestingly, disordered-phase regions showed the increase of both the conductivity and noise source density at an increased bias voltage condition. Such an increase of noise source densities could be attributed to the defect creation in the polymer chains induced by injected carriers. In addition, we found that the ordered-phase regions exhibited rather large increase in the conductivity and noise source density under light illuminations, which was attributed to the release of charge carriers trapped in rather deep traps. The direct imaging capability of noise sources via our strategy provides valuable insights about noise sources in conducting polymer channels. Thus, our strategy can be a powerful tool for basic research about electrical noises and should have a significant impact on modern electronics research.

Acknowledgements

This work was supported by BioNano Health-Guard Research Center funded by the Ministry of Science, ICT & Future Planning (MSIP) of Korea as Global Frontier Project (No. H-GUARD_2013M3A6B2078961). S.H. also acknowledges the support from NRF grants (Nos. 2013M3C8A3078813, 2014M3A7B4051591).

Notes and references

1 A. A. Balandin, *Nature Nanotech.*, 2013, **8**, 549.
2 X. Xie, D. Sarkar, W. Liu, J. Kang, O. Marinov, M. J. Deen, K. Banerjee, *ACS Nano*, 2014, **8**, 5633.
3 D. Lachance-Quirion, S. Tremblay, S. A. Lamarre, V. Methot, D. Gingras, J. C. Lemyre, M. Pioro-Ladriere, C. N. Allen, *Nano Lett.*, 2014, **14**, 882.
4 W. H. Pitchford, H.-J. Kim, A. P. Ivanov, H.-M. Kim, J.-S. Yu, R. J. Leatherbarrow, T. Albrecht, K.-B. Kim, J. B. Edel, *ACS Nano*, 2015, **9**, 1740.
5 Y. Kim, H. Song, D. Kim, T. Lee, H. Jeong, *ACS Nano*, 2010, **4**, 4426.
6 M. G. Sung, H. Lee, K. Heo, K.-E. Byun, T. Kim, D. H. Seo, S. Seo, S. Hong, *ACS Nano*, 2011, **5**, 8620.
7 A. A. Kaverzin, A. S. Mayorov, A. Shytov, D. W. Horsell, *Phys. Rev. B*, 2012, **85**, 075435.

8 G. Xu, C. M. Torres, Y. Zhang, F. Liu, E. B. Song, M. Wang, Y. Zhou, C. Zeng, K. L., *Nano Lett.*, 2010, **10**, 3312.
9 H. Lee, M. Lee, S. Namgung, S. Hong, *ACS Nano*, 2010, **4**, 7612.
10 A. T. Williams, P. Farrar, A. J. Gallant, D. Atkinson, C. Groves, *J. Mater. Chem. C*, 2014, **2**, 1742.
11 M. J. Deen, O. Marinov, J. Yu, S. Holdcroft, W. Woods, *IEEE Trans. Electron Devices*, 2001, **48**, 1688.
12 H. Kang, L. Jagannathan, V. Subramanian, *Appl. Phys. Lett.*, 2011, **99**, 062106.
13 G. Landi, C. Barone, A. D. Sio, S. Pagano, H. C. Neitzert, *Appl. Phys. Lett.*, 2013, **102**, 223902.
14 J. Planes, A. Francois, *Phys. Rev. B*, 2004, **70**, 184203.
15 J. Rivnay, S. C. B. Mannsfeld, C. E. Miller, A. Salleo, M. F. Toney, *Chem.Rev.*, 2012, **112**, 5488.
16 A. J. Heeger, *Rev. Mod. Phys.*, 2001, **73**, 681.
17 O. D. Jurchescu, B. H. Hamadani, H. D. Xiong, S. K. Park, S. Subramanian, N. M. Zimmerman, J. E. Anthony, T. N. Jackson, D. J. Gundlach, *Appl. Phys. Lett.*, 2008, **92**, 132103.
18 J. Rivnay, L. H. Jimison, J. E. Northrup, M. F. Toney, R. Noriega, S. Lu, T. J. Marks, A. Facchetti, A. Salleo, *Nature Mater.*, 2009, **8**, 952.
19 R. Noriega, J. Rivnay, K. Vandewal, F. P. V. Koch, N. Stingelin, P. Smith, M. F. Toney, A. Salleo, *Nature Mater.*, 2013, **12**, 1038.
20 H. T. Nicolai, M. Kuik, G. A. H. Wetzelaer, B. de Boer, C. Campbell, C. Risko, J. L. Bredas, P. W. M. Blom, *Nature Mater.*, 2012, **11**, 882 - 887.
21 W. Graupner, G. Leditzky, G. Leising, U. Scherf, *Phys. Rev. B*, 1996, **54**, 7610.
22 C. McNeill, *J. Polym. Sci. Part B: Polym. Phys.*, 2011, **49**, 909.
23 L. Ke, X. Y. Zhao, R. S. Kumar, S. J. Chua, *IEEE Electron Device Lett.* 2006, **27**, 555.
24 J. L. Luria, K. A. Schwarz, M. J. Jaquith, R. G. Hennig, J. A. Marohn, *Adv. Mater.*, 2011, **23**, 624.
25 C.-Y. Liu, S.-A. Chen, *Macromol. Rapid. Commun.*, 2007, **28**, 1743.
26 M. Jaquith, E. M. Muller, J. A. Marohn, *J. Phys. Chem. B*, 2007, **111**, 7711.
27 L. S. C. Pingree, B. A. MacLeod, D. S. Ginger, *J. Phys. Chem. C* 2008, **112**, 7922.
28 Q. Ferreira, G. Bernardo, A. Charas, L. Alcacer, J. Morgado, *J. Phys. Chem. C* 2010, **114**, 572.
29 E. Aharon, A. Albo, M. Kalina, G. L. Frey, *Adv. Funct. Mater.*, 2006, **16**, 980.
30 S. Shekhar, E. Aharon, N. Tian, F. Galbrecht, U. Scherf, E. Holder, G. L. Frey, *Chem. Phys. Chem.*, 2009, **10**, 576.
31 M. Engelson, Modern Spectrum Analyzer Theory and Applications, Artech House, **1984**.
32 P. Brenner, L. –M. Fleig, X. Liu, A. Welle, S. Brase, *J. Polym. Sci. Part B: Polym. Phys.*, 2015, **53**, 1029.
33 M.-C. Chen, W.-C. Hung, A.-C. Su, S.-H. Chen, S.-A. Chen, *J. Phys. Chem. B* 2009, **113**, 11124.
34 B. J. Schwartz, *Annu. Rev. Phys. Chem.*, 2003, **54**, 141.
35 M. Ariu, M. Sims, M. D. Rahn, J. Hill, A. M. Fox, D. G. Lidzey, M. Oda, J. Cabanillas-Gonzalez, D. D. C. Bradley, *Phys. Rev. B*, 2003, **67**, 195333.
36 K. P. Puntambekar, P. V. Pesavento, C. D. Frisbie, *Appl. Phys. Lett.*, 2003, **83**, 5539.
37 P. Prins, F. C. Grozema, B. S. Nehls, T. Farrell, U. Scherf, L. D. A. Siebbeles, *Phys. Rev. B*, 2006, **74** 113203.
38 H. –Y. Nie, M. J. Walzak, B. Berno, N. S. McIntyre, *Appl. Surf. Sci.*, 1999, **144-145** 627.
39 G. Haugstad, W. L. Gladfelter, R. R. Jones, *J. Vac. Sci. Technol. A*, 1996, **14** 1864.
40 B. Lin, L. Qiu, B. Qiu, Y. Peng, F. Yan, *Macromolecules*, 2011, **44**, 9642.
41 M. Ranger, M. Leclerc, *Macromolecules*, 1999, **32**, 3306.
42 A. Carbone, B. K. Kotowska, D. Kotowski, *Phys. Rev. Lett.*, 2005, **95**, 236601.
43 A. Carbone, C. Pennetta, L. Reggiani, *Appl. Phys. Lett.*, 2009, **95**, 233303.
44 R. Jayaraman, C. G. Sodini, *IEEE Trans. Electron Devices*, 1989, **36**, 1773.
45 Z. Celik-Butler, T. Y. Hsiang, *IEEE Trans. Electron Devices*, 1988, **35**, 1651.
46 F. N. Hooge, T. G. M. Kleinpenning, L. K. J. Vandamme, *Rep. Prog. Phys.*, 1981, **44**, 479.
47 C. -K. Yang, C. -M. Yang, H.-H. Liao, S. -F. Horng H. -F. Meng, *Appl. Phys. Lett.*, 2007, **91**, 093504.
48 J. L. Bredas, G. B. Street, *Acc. Chem. Res.*, 1985, **18**, 309.
49 O. Bubnova, Z. U. Khan, H. Wang, S. Braun, D. R. Evans, M. Fabretto, P. Hojati-Talemi, D. Dagnelund, J.-B. Arlin, Y. H. Geerts, S. Desbief, D. W. Breiby, J. W. Andreasen, R. Lazzaroni, W. M. Chen, I. Zozoulenko, M. Fahlman, P. J. Murphy, M. Berggren, X. Crispin, *Nature Mater.*, 2014, **13** 190.